ANTIOXIDANTS & REDOX SIGNALING
Volume 3, Number 5, 2001
Mary Ann Liebert, Inc.

Forum Review

Catalytic Control of Redox Reactivities of Coenzyme Analogs by Metal Ions

SHUNICHI FUKUZUMI[1] and SHINOBU ITOH[2]

ABSTRACT

Redox coenzymes and analogs have their own redox reactivities for both thermal and photochemical redox reactions. The redox activities of coenzymes can be tuned by using metal ions that can bind the redox coenzymes and analogs. Quantitative measure to determine the Lewis acidity of a variety of metal ions is given in relation to the catalytic reactivities. The mechanistic viability of metal ion catalysis in redox reactions of coenzyme analogs is described by showing a number of examples of both thermal and photochemical reactions that are made possible to proceed by controlling the redox reactivities of coenzymes with metal ions. Antioxid. Redox Signal. 3, 807–824.

INTRODUCTION

METAL IONS ACTING AS LEWIS ACIDS have played a pivotal role in promoting various reactions of synthetic value because of the high reactivities and selectivities achieved under the mild reaction conditions (57, 62, 73, 75, 86). Metal ions and the salts acting as Lewis acids can also promote free radical reactions (38, 65, 72, 77) and electron transfer reactions (12, 13, 15, 16). The Lewis acid-promoted reactions are believed to proceed through the coordination of a Lewis acid to a lone pair of heteroatoms, such as an oxygen atom of carbonyl compounds and a nitrogen atom of imines (57, 62, 73, 75, 86). The essential roles of metal ions have also been well-recognized in a variety of enzymatic functions (41, 54, 59). Considerable efforts have so far been made to not only detect, but also chemically and functionally characterize, trace elements or otherwise inconspicuous metal ions in various enzymatic systems. As most redox coenzymes contain a lone pair of heteroatoms, which can coordinate to metal ions, the binding of metal ions to redox coenzymes is expected to result in significant change in the redox reactivities.

This review is generally intended to focus on the catalytic control of redox reactivities of coenzyme analogs by metal ions rather than on the direct relevance to the specific enzymatic process. Considering only two-electron reduction of a coenzyme analog (A), the reduction and protonation give nine species at different oxidation and protonation states as shown in Scheme 1. Each species can have an interaction with a variety of metal ions (M^{n+}), and such an interaction can control each redox and protonation step in Scheme 1.

The catalytic reactivities of metal ions are cer-

[1]Department of Material and Life Science, Graduate School of Engineering, Osaka University, CREST, JAPAN Science and Technology Corporation, 2-1 Yamada-oka, Suita, Osaka 565-0871, Japan.
[2]Department of Chemistry, Graduate School of Science, Osaka City University, 3-3-138 Sugimoto, Sumiyoshi-ku, Osaka 558-8585, Japan.

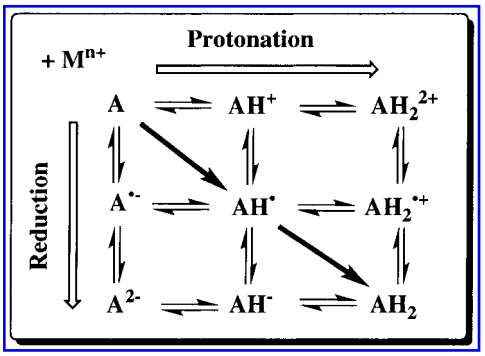

Scheme 1.

tainly related to the Lewis acidity of metal ions used to promote the reactions. Charges and ion radii are important factors to determine the Lewis acidity of metal ions. In the beginning, quantitative measure to determine the Lewis acidity of a variety of metal ions is described in relation to the catalytic reactivities. Then the mechanistic viability is described by showing a number of examples of both thermal and photochemical reactions of coenzyme analogs that are promoted by metal ions.

QUANTITATIVE MEASURE OF THE LEWIS ACIDITY OF METAL IONS

The catalytic reactivity of metal ions in redox reactions should be related to the binding strength of metal ions with redox active reactants. Unfortunately, there are only limited number of formation constants for metal ion complexes with carbonyl compounds, and thus, it had been difficult to know the difference in the Lewis acidity of a variety of metal ions (M^{n+}) in a quantitative manner. However, it has recently been shown that the binding energies of a variety of metal ions with superoxide ion ($O_2^{\bullet-}$) can be readily derived from the g_{zz}-values of the electron spin resonance (ESR) spectra of the superoxide–metal ion complexes ($O_2^{\bullet-}$-M^{n+}), providing the quantitative measure of Lewis acidity of the metal ions (*vide infra*) (17).

The g_{zz} value of $O_2^{\bullet-}$-M^{n+} gives valuable information concerning the binding strength of $O_2^{\bullet-}$-M^{n+}. The deviation of the g_{zz} value from the free spin value ($g_e = 2.0023$) is caused by the spin-orbit interaction as given by Eq. 1 (55, 87)

$$g_{zz} = g_e + \sqrt{\frac{\lambda^2}{\lambda^2 + \Delta E^2}} \qquad (1)$$

where λ is the spin-orbit coupling constant (0.014 eV) (56) and ΔE is the energy splitting of π_g levels due to the complex formation between $O_2^{\bullet-}$ and M^{n+}. Under the conditions that $\Delta E >> \lambda$, Eq. 1 is rewritten by Eq. 2

$$\Delta E = (g_{zz} - g_e)/2\lambda \qquad (2)$$

in which the ΔE value is readily obtained from the deviation of the g_{zz} value from the free spin value. The ΔE value increases generally in order: monovalent cations (M^+) < divalent cations (M^{2+}) < trivalent cations (M^{3+}) (17). The ΔE value also increases with decreasing ion radius when the oxidation state of the metal ion is the same. The same trend has been reported for $O_2^{\bullet-}$ adsorbed on the surface of various metal oxides (8, 60). Scandium ion which has the smallest ion radius among the trivalent metal cations, gives the largest ΔE value, and this indicates that the binding energy between Sc^{3+} and $O_2^{\bullet-}$ is the strongest (17). In the case of $O_2^{\bullet-}$-Sc^{3+}, an "end-on" coordination form of $^{\bullet}$O-O$^-$-Sc^{3+} is indicated by the hyperfine splitting of two different ^{17}O atoms ($I = 5/2$) in which the electron spin is more localized at the terminal oxygen (60%) (32). This is confirmed by the density function theory calculation using the spin-restricted B3LYP functional and the 6-311++G(3d,3p) basis set for the open shell $O_2^{\bullet-}$-Sc^{3+}, which gives more localized spin density at the terminal oxygen (65%) (17). The calculated O-O distance decreases in order: $O_2^{\bullet-}$ (1.343 Å) > $O_2^{\bullet-}$-Li^+ (1.309 Å) > $O_2^{\bullet-}$-Mg^{2+} (1.297 Å) > $O_2^{\bullet-}$-Sc^{3+} (1.211 Å) as the ΔE value increases (17).

The applicability of ΔE to predict the promoting effects of M^{n+} in electron transfer reactions has been nicely shown in M^{n+}-promoted electron transfer from (TPP)Co (TPP = tetraphenylporphyrin dianion) to *p*-benzoquinone (Q) (Eq. 3) as well as O_2 in acetonitrile (MeCN) at 298 K (17).

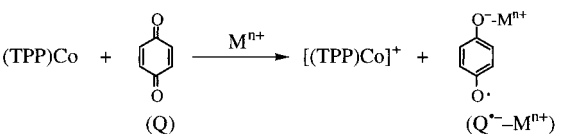

(3)

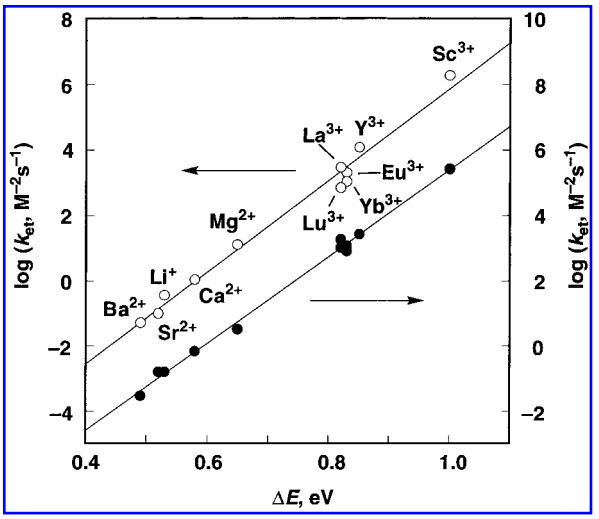

FIG. 1. Plots of log k_{et} versus ΔE in M^{n+}-catalyzed electron transfer from (TPP)Co to O_2 (○) and *p*-benzoquinone (●).

In the absence of metal ion, no electron transfer from (TPP)Co to Q or O_2 occurs because the electron transfer is highly endergonic judging from the one-electron oxidation potential of (TPP)Co [$E^0_{ox} = 0.35$ V versus standard calomel electrode (SCE) in MeCN] and the one-electron reduction potential of Q ($E^0_{red} = -0.51$ V versus SCE) (17) or O_2 ($E^0_{red} = -0.83$ V versus SCE) (74). The promoting effects of metal ions in electron transfer reduction of substrates have been ascribed to the binding of metal ions to the radical anions produced in the electron transfer reactions (13–16). There is a *striking linear correlation* between the rate constants (log k_{et}) of M^{n+}-promoted electron transfer from (TPP)Co to Q or O_2 and ΔE of $O_2^{\cdot -}$-M^{n+} derived from the g_{zz} values as shown in Fig. 1. The remarkable correlation spans a range of almost 10^7 in the rate constant. The slope of the linear correlation between log k_{et} for M^{n+}-promoted electron transfer from (TPP)Co to O_2 and ΔE is obtained as 14.0, which is close to the value of $1/2.3kT$ (= 16.9, where k is the Boltzmann constant and $T = 298$ K) (17). The slope (13.3) for Q (filled circles) is nearly the same as the slope (14.0) for O_2 (open circles). This means that the variation of ΔE is well reflected in the difference in the activation free energy for the M^{n+}-promoted electron transfer from (TPP)Co to Q as well as O_2. The stronger the binding of M^{n+} with $O_2^{\cdot -}$, the larger will be the promoting effects of M^{n+}. Thus, ΔE is regarded as a good measure of the binding energies in the $O_2^{\cdot -}$-M^{n+} complexes, which can be used as a quantitative measure of Lewis acidity of the metal ion (17).

NADH ANALOGS

Hydride transfer

Most biological redox reactions are mediated by redox coenzymes such as NAD(P)H (NAD^+ = nicotinamide adenine dinucleotide; $NADP^+$ = nicotinamide adenine dinucleotide phosphate; NADH, NADPH = the reduced forms of NAD^+ and $NADP^+$, respectively). The NAD(P)H coenzymes act as a source of two electrons and a proton, thus formally transferring a hydride ion to a substrate (Eq. 4) (80).

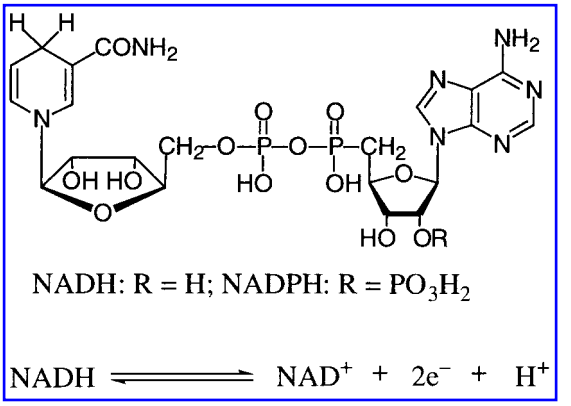

(4)

The effects of metal ions such as Mg^{2+} and Zn^{2+} ions on hydride transfer reactions from NADH model compounds to substrates have attracted considerable interest in relation to the role of metal ions in the redox reactions of nicotinamide coenzymes (13, 78).

The effects of Mg^{2+} on hydride transfer reactions from a typical NADH model compound, 1-benzyl-1,4-dihydronicotinamide (BNAH), to substrates have been shown to be rather complex (22, 27). When a relatively strong oxidant such as 7,7,8,8-tetracyano-*p*-quinodimethan (TCNQ) is used as a hydride acceptor, the addition of Mg^{2+} to the BNAH-TCNQ system in anhydrous MeCN causes a significant decrease in the reaction rate (22). The rate constant of hydride transfer from BNAH to TCNQ decreases with an increase in

$[Mg^{2+}]$ to reach a constant value that is 23 times smaller than the value in the absence of Mg^{2+} (22). Such a retarding effect of Mg^{2+} is well interpreted by the 1:1 complex formation between BNAH and Mg^{2+} (Eq. 5), which reacts with TCNQ at a much slower rate than BNAH (Eqs. 6 and 7) (22).

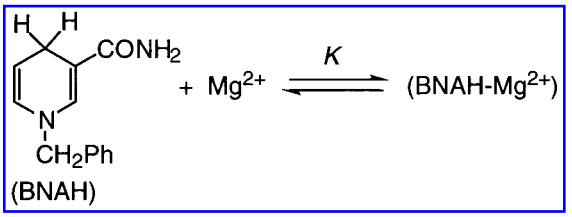

(5)

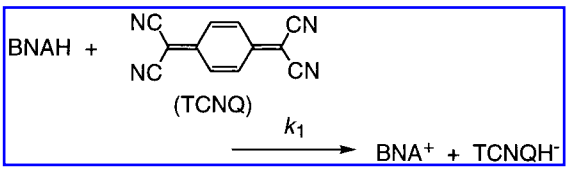

(6)

$$\text{BNAH-Mg}^{2+} + \text{TCNQ} \xrightarrow[\text{slow}]{k_2} \text{BNA}^+ + \text{Mg}^{2+} + \text{TCNQH}^- \quad (7)$$

In such a case, the dependence of the observed second-order rate constant k_{obs} on $[Mg^{2+}]$ is given by Eq. 8

$$k_{obs} = (k_1 + k_2K[Mg^{2+}])/(1 + K[Mg^{2+}]) \quad (8)$$

where k_1 and k_2 are the rate constants of free BNAH (Eq. 6) and the Mg^{2+} complex (Eq. 7), respectively. The K value for the complex formation between BNAH and Mg^{2+} is determined as $1.1 \times 10^4\ M^{-1}$ from the dependence of k_{obs} on $[Mg^{2+}]$ (Eq. 8), agreeing well with the value determined by the spectroscopic change of BNAH due to the complex formation with Mg^{2+} ($1.2 \times 10^4\ M^{-1}$) (22). As there is no interaction between $TCNQ^{\cdot -}$ and Mg^{2+}, the reduction potential of TCNQ is not affected by the presence of Mg^{2+} (27). On the other hand, the one-electron oxidation potential of BNAH (E^0_{ox} = 0.57 V versus SCE) in MeCN is significantly shifted to the positive direction due to the complexation with Mg^{2+} (0.80 V versus SCE) (29).

It is now well established that the hydride transfer from NADH analogs to strong oxidants such as TCNQ proceeds via sequential electron–proton–electron transfer in which the initial electron transfer to give the radical ion pair ($BNAH^{\cdot +}$ $TCNQ^{\cdot -}$) is in equilibrium with the charge transfer complex (BNAH TCNQ) and the proton transfer from $BNAH^{\cdot +}$ to $TCNQ^{\cdot -}$ is the rate-determining step (25, 29, 33). Thus, a positive shift in the E^0_{ox} value of BNAH due to the complexation with Mg^{2+} results in a smaller equilibrium constant for the radical ion pair formation, leading to a decrease in the overall rate of hydride transfer from BNAH to TCNQ as observed experimentally.

When TCNQ is replaced by a weaker oxidant such as 2,6-dichloro-*p*-benzoquinone, the Mg^{2+} ion shows both retarding and accelerating effects on the hydride transfer reaction depending on the Mg^{2+} concentration, as shown in Fig. 2, where the observed second-order rate constant (k_{obs}) decreases sharply from the value in the absence of Mg^{2+} ($7.5 \times 10\ M^{-1}\ s^{-1}$) with an increase in $[Mg^{2+}]$ at low concentrations ($<<0.10\ M$), whereas the k_{obs} value increases at the higher concentrations (>ca. 0.10 *M*) (27). The sharp decrease in the rate constant from the value in the absence of Mg^{2+} to the value in the presence of Mg^{2+} (0.10 *M*) is ascribed to the positive shift of the E^0_{ox} value of BNAH from the value in the absence of Mg^{2+} as in the case of TCNQ. In contrast to the case of TCNQ, however, the reduction potential (E^0_{red}) of 2,6-dichloro-*p*-benzoquinone is also shifted to the positive direction due to the complexation of Mg^{2+} with the semiquinone radical anion (27).

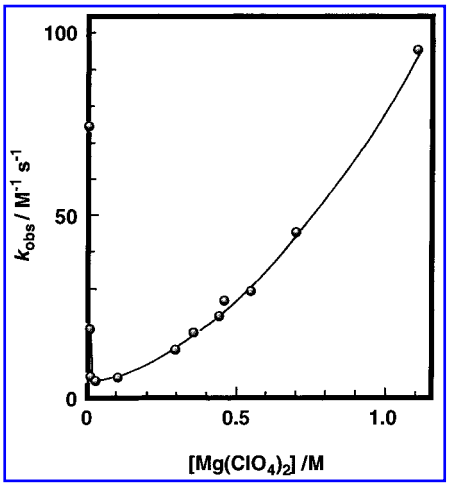

FIG. 2. Plot of k_{obs} versus $[Mg(ClO_4)_2]$ for the hydride transfer reaction from BNAH to 2,6-dichloro-*p*-benzoquinone in the presence of $Mg(ClO_4)_2$ in MeCN at 298 K (27).

In the presence of a large concentration of Mg^{2+} (*e.g.*, 1.6 *M*), the positive shift of the E^0_{red} value of the quinone (0.21 V) becomes larger than the corresponding positive shift of BNAH (0.18 V) (27). This is the reason for the recovery of the reactivity at the high Mg^{2+} concentration as compared with that in the absence of Mg^{2+} (Fig. 2). Thus, the change of the k_{obs} values depending on $[Mg^{2+}]$ is caused by the corresponding change in the free energy change of electron transfer from BNAH to the substrate in the presence of Mg^{2+}, ΔG^0_{et}*, which is given by $F(E^0_{ox}* - E^0_{red}*)$, where * denotes the value in the presence of Mg^{2+}. Such a dependence of k_{obs} on ΔG^0_{et}* has generally been shown for various Q derivatives at different Mg^{2+} concentrations (27). This indicates that electron transfer from BNAH to Q in the charge-transfer complex formed between BNAH and Q is the rate-determining step that determines the overall reactivity of the hydride transfer reactions in the absence and presence of Mg^{2+}, as shown in Scheme 2 (27). The electron transfer from BNAH to Q is accelerated by the complexation of Mg^{2+} with $Q^{\cdot -}$, whereas the complexation of Mg^{2+} with BNAH retards the electron transfer. With an increase in the Mg^{2+} concentration, not only one Mg^{2+} but also two Mg^{2+} ions can form the complex with $Q^{\cdot -}$, resulting in a second-order dependence of k_{obs} with respect to $[Mg^{2+}]$, as shown in Fig. 2 (27). The electron transfer is followed by the proton transfer from $BNAH^{\cdot -}$ to the Mg^{2+} complex of $Q^{\cdot -}$, and the subsequent electron transfer from $BNA^{\cdot}$ to the Mg^{2+} complex of $QH^{\cdot}$ occurs efficiently because of the largely negative oxidation potential of $BNA^{\cdot}$ (−1.1 V versus SCE) (29). The observed primary kinetic isotope effects, k_H/k_D have well been analyzed as those on the proton transfer $BNAH^{\cdot +}$ to the Mg^{2+} complex of $Q^{\cdot -}$ (27).

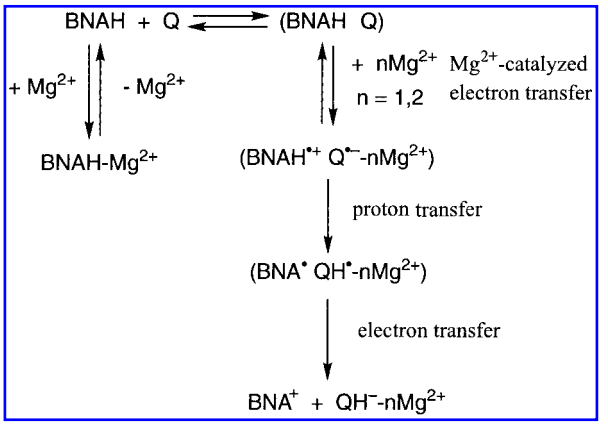

Scheme 2.

Semiquinone radical anion–metal ion complexes

The transient electronic spectra of semiquinone radical anion in the presence of different concentrations of Mg^{2+} are obtained by measuring the change in initial absorbance at various wavelengths with use of a stopped-flow spectrophotometer (18). The transient absorption spectrum of $Q^{\cdot -}$ in the presence of 1.0×10^{-2} *M* Mg^{2+} (λ_{max} = 590 nm) is significantly red-shifted as compared with that in the absence of Mg^{2+} (λ_{max} = 422 nm) (21). Further addition of Mg^{2+} results in a blue shift to λ_{max} = 415 nm with a clean isosbestic point (18). Such spectroscopic changes indicate the formation of complexes between $Q^{\cdot -}$ and Mg^{2+}, which requires two steps. The first step is the formation of a 1:1 complex ($Q^{\cdot -}$-Mg^{2+}) and the second step is an additional addition of Mg^{2+} to form a 1:2 complex ($Q^{\cdot -}$-$2Mg^{2+}$), as shown in Eqs. 9 and 10, respectively (18).

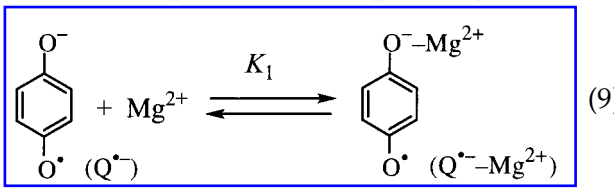

(9)

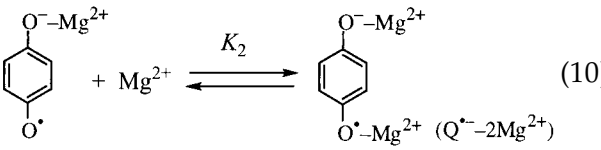

(10)

Transient electronic spectra of the 1:1 and 1:2 complexes are also observed in the electron transfer reduction of 2,5-dichloro-*p*-benzoquinone and 2,5-dimethyl-*p*-benzoquinone (18). The formation constant K_2 for the 1:2 complex determined from the transient electronic spectra decreases with a decrease in the electron-donating ability of X-$Q^{\cdot -}$ (X × 2,5-Me_2 > H > 2,5-Cl_2) (18). The formation of such complexes has also been confirmed by the ESR spectra observed in the electron-transfer re-

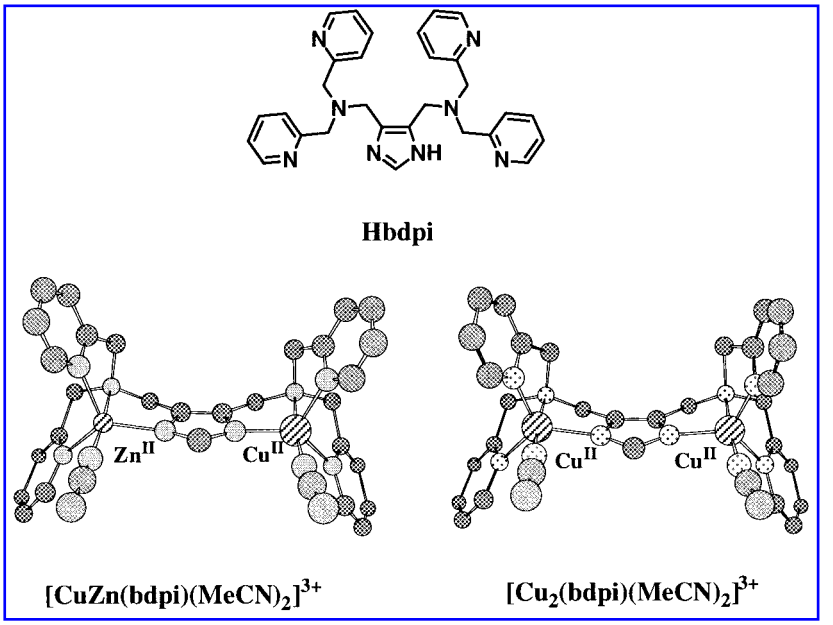

FIG. 3. Structures of SOD models (71).

duction of Q in the presence of Mg^{2+} by applying a rapid-mixing ESR technique (18).

The complex formation between $Q^{\cdot -}$ and Zn^{2+} has also been shown to play an essential role in the reduction of $Q^{\cdot -}$ by imidazolate-bridged Cu^{II}-Zn^{II} heterodinuclear and Cu^{II}-Cu^{II} homodinuclear complexes, $[CuZn(bdpi)(MeCN)_2]^{3+}$ and $[Cu_2(bdpi)(MeCN)_2]^{3+}$, where bdpi = 4,5-bis[di(2-pyridylmethyl)aminomethyl]imidazole (Fig. 3) (69), which can act as a copper-zinc superoxide dismutase (Cu,Zn-SOD) model (71). This enzyme catalyzes a very rapid two-step dismutation of toxic superoxide ($O_2^{\cdot -}$) to dioxygen (O_2) and hydrogen peroxide (H_2O_2) through an alternate reduction and oxidation of the active-site copper ion (5, 10–12). The complexation of $Q^{\cdot -}$ with Zn^{2+} in $[Cu^{I}(Q)Zn^{II}(bdpi)]^{2+}$ facilitates an intramolecular electron transfer from the Cu^{I} center, which is produced by an electron transfer from $Q^{\cdot -}$ to the Cu^{II} center of $[Cu^{II}(Q)Zn^{II}(bdpi)]^{3+}$, to $Q^{\cdot -}$ bound to Zn^{2+} as shown in Scheme 3 (69). In the case of $[Cu_2(bdpi)]^{3+}$, however, there is no Zn^{2+} available to facilitate the reduction of $Q^{\cdot -}$, because both Cu^{II} ions are reduced to Cu^{I} by the reaction with $Q^{\cdot -}$. In an aprotic solvent such as propionitrile, the final product of the stoichiometric disproportionation of $Q^{\cdot -}$ is $[Cu^{I}(Q)Zn^{II}(Q^{2-})(bdpi)]^{+}$ (Scheme 3), which was confirmed by the electron spray ionization mass spectrum (69). In the presence of H^{+}, $[CuZn(bdpi)]^{3+}$ can act as a catalyst for the disproportionation of $Q^{\cdot -}$ to Q and QH_2 (see broken arrow in Scheme 3). The $Q^{\cdot -}$-Zn^{2+} complex has been detected spectroscopically by using the mononuclear Zn^{2+} complex of $[Zn(MeIm(Py)_2)(MeCN)]^{2+}$, where $MeIm(Py)_2$ = (1-methyl-4-imidazolylmethyl) bis(2-pyridylmethyl)amine (69). The absorption band at 570 nm of the Zn^{2+}-$Q^{\cdot -}$ complex which is slightly blue-shifted as compared with the Mg^{2+} complex in Eq. 9 (λ_{max} = 590 nm), is assigned to a π-π^* transition of $[Zn(Q^{\cdot -})(MeIm(Py)_2)]^{+}$ (69). In Scheme 3, Zn^{2+} facilitates both the oxidation and reduction of $Q^{\cdot -}$. Essentially the same mechanism may be applied to the disproportionation of $O_2^{\cdot -}$ catalyzed by Zn,Cu-

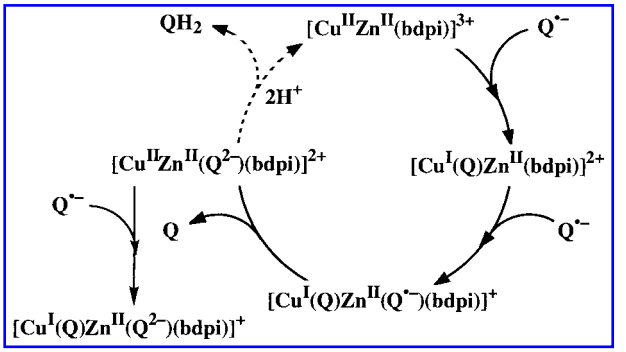

Scheme 3.

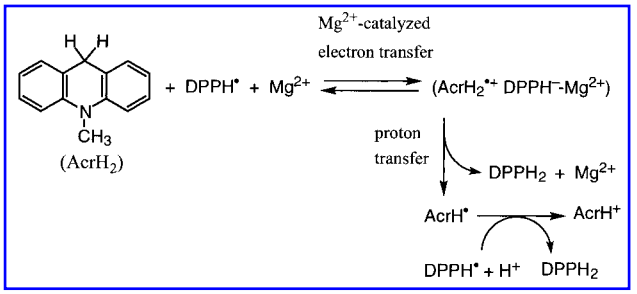

Scheme 4.

SOD, because the coordination of $O_2^{\cdot -}$ to Zn^{2+} is also essential for the reduction of $O_2^{\cdot -}$ by the Cu^{I} center (70, 71).

Hydrogen transfer

Metal ions can also promote hydrogen transfer from an NADH analog to neutral radicals via metal ion-catalyzed electron transfer (30). Hydrogen transfer from 10-methyl-9,10-dihydroacridine ($AcrH_2$) to a stable radical, 1,1-diphenyl-2-picrylhydrazyl ($DPPH^{\cdot}$), proceeds via electron transfer from $AcrH_2$ to $DPPH^{\cdot}$, which is catalyzed by the presence of Mg^{2+}, followed by proton transfer from $AcrH_2^{\cdot +}$ to $DPPH^-$ to yield $DPPH_2$ (Scheme 4) (30). The resulting acridinyl radical ($AcrH^{\cdot}$) is a much stronger reductant than $AcrH_2$, judging from the more negative oxidation potential (−0.43 V) (29) than that of $AcrH_2$ (0.81 V) (31), and thereby $AcrH^{\cdot}$ can readily transfer an electron to another $DPPH^{\cdot}$ molecule to yield $AcrH^+$ (Scheme 4). The primary kinetic isotope effect determined as $k_H/k_D = 3.0$ at 323 K is ascribed to the proton transfer from $AcrH_2^{\cdot +}$ to $DPPH^-$ (30). The electron-transfer process is favored in the case of $DPPH^{\cdot}$, which has the positive one-electron reduction potentials (0.24 V). The significant steric effect of the bulky substituents of $DPPH^{\cdot}$ also contributes to favor the electron-transfer pathway, because no significant interaction is required for the electron-transfer process, as compared with an alternative direct hydrogen-transfer process, which requires the close contact of the reactants (30).

On the other hand, phenoxyl radicals derived from tyrosine and its derivatives have been reported to participate in a variety of enzymatic catalysis, such as in class I ribonucleotide reductase, photosystem II, prostaglandin H synthase, galactose oxidase, cytochrome *c* oxidase, bovine liver catalase, and DNA photolyase (3, 53, 61, 81). In these cases, the tyrosine radical mainly acts as a hydrogen atom acceptor to induce C—H bond activation of the substrate, which is the initial step of the above enzymatic reactions (81). Metal ions bound to a tyrosine radical have been shown to enhance the radical stability as well as control reactivity of the phenoxyl radical species. One of the most well documented examples of such systems is galactose oxidase (44), where tyrosine radical coordinated to copper(II) acts as an active species for the oxidation of primary alcohols to the corresponding aldehydes (84). Extensive efforts have so far been made not only to mimic the biochemical reactivity of galactose oxidase, but also to provide valuable insight into the general aspects of structures, physicochemical properties, and functions of phenoxyl radical complexes with a series of transition-metal ions (39, 49, 79).

Reactivity of phenoxyl radicals in the hydrogen-transfer reactions from $AcrH_2$ and its 9-substituted derivatives (AcrHR, R = Me, Et, and Ph) has also been shown to be controlled by metal ions (52). Phenolate complexes of a series of alkaline earth metal ions, as well as monovalent cations such as Na^+ and K^+, have been prepared by using 2,4-di-*tert*-butyl-6-(1,4,7,10-tetraoxa-13-azacyclopentadec-13-ylmethyl)phenol (**L1H**) and 2,4-di-*tert*-butyl-6-(1,4,7,10,13-pentaoxa-16-azacyclooctadec-16-ylmethyl)phenol (**L2H**) (52).

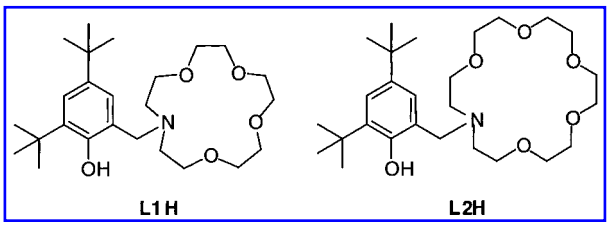

Crystal structures of the Mg^{2+} and Ca^{2+} complexes of $\mathbf{L1}^-$, as well as the Ca^{2+} and Sr^{2+} complexes of $\mathbf{L2}^-$, were determined by x-ray crystallographic analysis, showing that the crown ether rings in the Ca^{2+} complexes are significantly distorted from planarity, whereas those in the Mg^{2+} and Sr^{2+} complexes are fairly flat (52). Figure 4 shows the x-ray structures of $[Mg(\mathbf{L1}^-)]^+$ and $[Ca(\mathbf{L1}^-)]^+$ as typical exam-

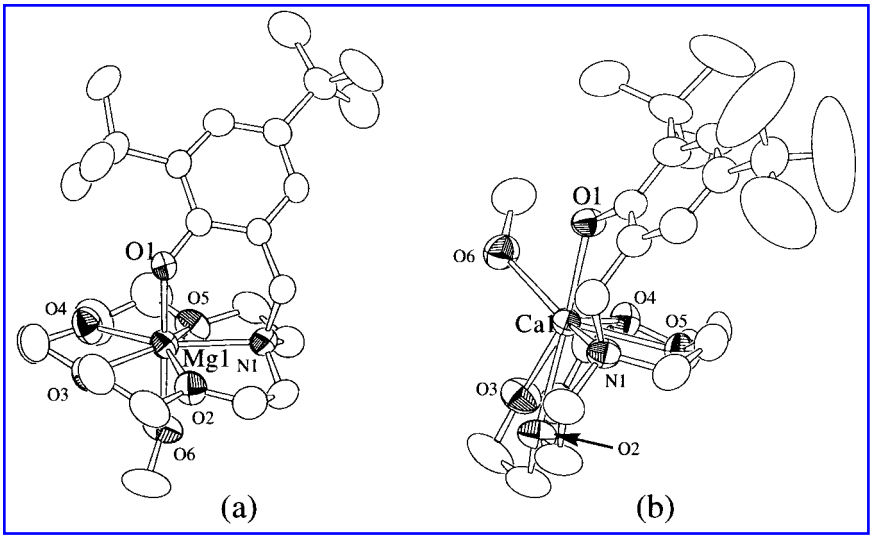

FIG. 4. ORTEP drawing of the cationic part of (a) [Mg(L1$^-$)-(CH$_3$OH)]BPh$_4$ and (b) [Ca(L1$^-$)(CH$_3$OH)]BPh$_4$ (52). The counter anions and hydrogen atoms are omitted for clarity.

ples. The phenoxyl radical complexes are successfully generated *in situ* by the oxidation of the phenolate complexes with $(NH_4)_2[Ce^{4+}(NO_3)_6]$ (ceric ammonium nitrate) (52). The hydrogen transfer reactions were performed at −40°C, where the disproportionation of the phenoxyl radical complexes was negligibly slow (52). The overall reaction consists of a formal hydrogen atom transfer from AcrHR to M(**Ln**$^{\bullet}$) to afford AcrR$^{\cdot}$ (R = H, D, Me, Et, or Ph) and M(**LnH**) and a subsequent electron transfer from the resulting AcrR$^{\cdot}$ to another M(**Ln**$^-$) generating AcrR$^+$ and M(**Ln**$^{\bullet}$) as shown in Scheme 5 (52). Relatively large primary kinetic isotope effects k_H/k_D = 4.9–12.5 were obtained when $AcrH_2$ is replaced by $AcrD_2$, confirming that the initial hydrogen atom transfer is the rate-determining step (52). Thus, the k_H values can be regarded as measure of H$^{\cdot}$-abstraction ability of the phenoxyl radical–metal complexes.

The k_H value increases in order: $Sr^{2+} < Ca^{2+} < Mg^{2+}$ with increasing Lewis acidity of metal ions, when the binding of metal ions to the phenoxyl radical becomes stronger (52). The $E_{1/2}$ values of the cation complexes of **L1**$^-$ or **L2**$^{2-}$ also increase in order: $Bu_4N^+ < K^+ < Na^+ < Ba^{2+} < Sr^{2+} < Ca^{2+} < Mg^{2+}$ (52). This order agrees with the Lewis acidity of cationic species derived from the superoxide ion complexes with cationic species (Fig. 1) (17). Thus, the stronger the Lewis acidity of metal ions, the more positive the $E_{1/2}$ value, *i.e.*, the stronger the oxidation ability of the complexes. In addition, the k_H/k_D value *increases* with increasing binding strength of metal ions to the phenoxyl radical in order: $Na^+ < Sr^{2+} < Ca^{2+} < Mg^{2+}$. This is completely opposite from what is expected for a one-step hydrogen-transfer reaction in which the primary kinetic deuterium isotope effects (k_H/k_D) should decrease with increasing binding strength of metal ions to the phenoxyl radical when the driving force of hydrogen transfer decreases (43). The large pri-

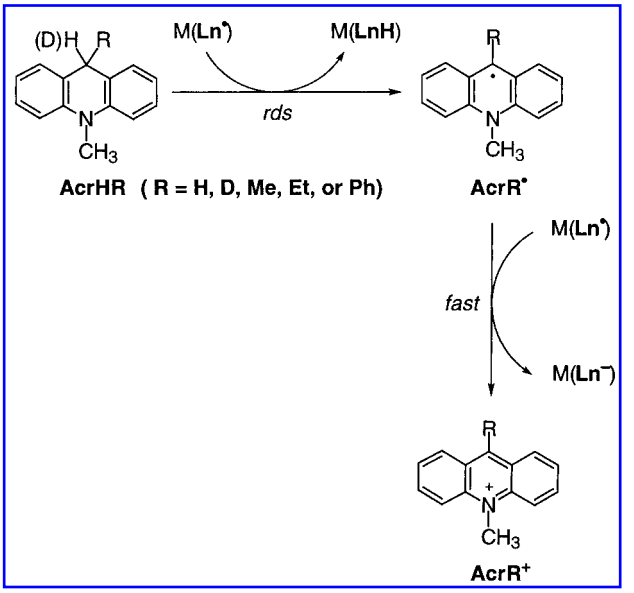

Scheme 5.

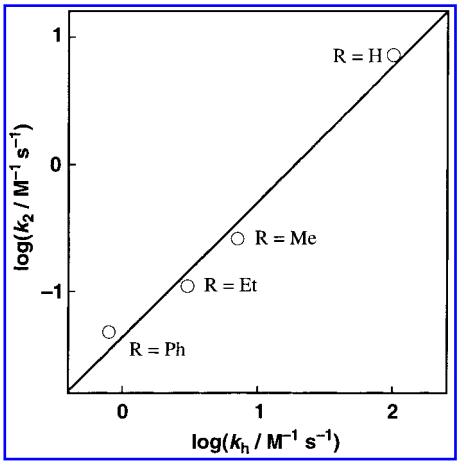

FIG. 5. Comparison of the rate constant (log k_H) of hydrogen transfer from AcrHR (R = H, Me, Et, and Ph) to Ca^{2+}(L1·) and the rate constant (log k_h) of hydride transfer from AcrHR to TCNE (52).

mary kinetic isotope effects (7.1–12.5) observed for alkaline earth metal−**L1**· complexes are consistent with those reported for proton transfer from $AcrH_2^{\cdot+}$ to semiquinone radical anions (7.2–10.4) (43). Furthermore, the reactivity of $AcrH_2$ toward the hydrogen-transfer reaction with the Ca^{2+}−**L1**· complex is diminished when $AcrH_2$ is replaced by AcrHR (R = Me, Et, and Ph). Such diminished reactivity of $AcrH_2$ is also observed for a hydride transfer reaction from AcrHR to tetracyanoethylene (TCNE), which has been shown to proceed via electron transfer from AcrHR to TCNE followed by proton transfer from $AcrHR^{\cdot+}$ to $TCNE^{\cdot-}$ (33). A parallel relationship between k_H values of hydrogen-transfer reactions from AcrHR to the Ca^{2+}−**L1**· complex and the k_H values (k_h: the rate constant of hydride transfer from AcrHR to TCNE) (33) is shown in Fig. 5. This indicates that the hydrogen transfer in Scheme 5 proceeds via sequential electron and proton transfer. The reactivity of electron and proton transfer processes are controlled by the complexation of metal ions with phenoxyl radicals.

Not only neutral radicals but also radical anions can abstract a hydrogen atom from an NADH analog BNAH (20). As is the case of the hydrogen transfer from BNAH to DPPH·, the hydrogen transfer from BNAH to 2,3-dicyano-5,6-dichloro-*p*-benzosemiquinone radical anion ($DDQ^{\cdot-}$) is followed by fast electron transfer from BNA· (E^0_{ox} = -1.1 V) to $DDQ^{\cdot-}$ (E^0_{red} = −0.31 V) to yield BNA^+, DDQ^{2-}, and $DDQH^-$ (20). The BNAH can also reduce *p*-chloranil radical anion ($Cl_4Q^{\cdot-}$), although the reactivity of $Cl_4Q^{\cdot-}$ ($k_{obs} = 1.1 \times 10^{-1}\ M^{-1}\ s^{-1}$) is much smaller than that of $DDQ^{\cdot-}$ ($1.1 \times 10\ M^{-1}\ s^{-1}$). The addition of $NaClO_4$ to the BNAH-$Cl_4Q^{\cdot-}$ system results in an increase in the rate of the hydrogen transfer. The k_{obs} value increases linearly with an increase in [$NaClO_4$], whereas no acceleration of the rates is observed in the presence of Bu_4NClO_4 (20). The significant accelerating effect of $NaClO_4$ on the hydrogen transfer from BNAH to $Cl_4Q^{\cdot-}$ is confirmed by the voltammetric study (20). The reduction peak potential of $Cl_4Q^{\cdot-}$ is significantly shifted to the positive direction in the presence of 0.10 *M* $NaClO_4$ as compared with the position in the presence of 0.10 *M* Bu_4NClO_4 (20). Such a positive shift in the presence of $NaClO_4$ indicates that the one-electron reduction of $Cl_4Q^{\cdot-}$ is accompanied by the complex formation of the one-electron reduced product (Cl_4Q^{2-}) with Na^+, because no effect of Na^+ was observed on the electronic spectrum of $Cl_4Q^{\cdot-}$. In fact, the redox couple of $Cl_4Q/Cl_4Q^{\cdot-}$ is unaffected by the presence of 0.10 *M* $NaClO_4$ as compared with that in the presence of 0.10 *M* Bu_4NClO_4 (20).

On the basis of the accelerating effect of Na^+ on the one-electron reduction of radical anions, combined with the observation of the large primary kinetic isotope effect (k_H/k_D = 22), the reaction mechanism of the Na^+-promoted hydrogen transfer from BNAH to $Cl_4Q^{\cdot-}$ is given by Scheme 6 (20). The initial electron transfer

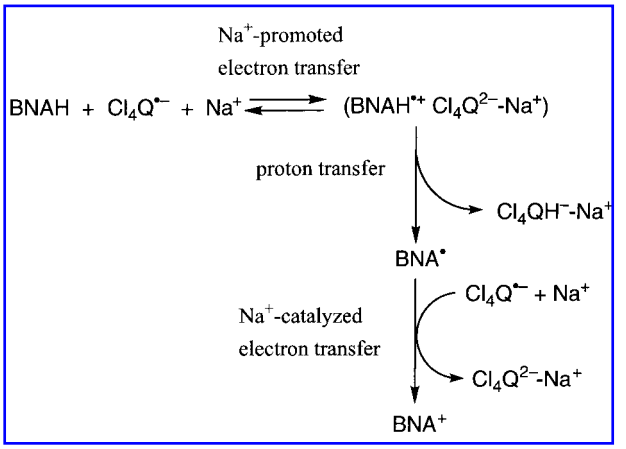

Scheme 6.

from BNAH to $Cl_4Q^{\cdot -}$ is accelerated by the presence of Na^+ due to the complexation with Cl_4Q^{2-}, followed by proton transfer from $BNAH^{\cdot +}$ to Cl_4Q^{2-}-Na^+ to yield $BNA^{\cdot}$ and Cl_4QH^-. The subsequent electron transfer from $BNA^{\cdot}$ to $Cl_4Q^{\cdot -}$ is fast to yield BNA^+ and Cl_4Q^{2-} (Scheme 6). According to Scheme 6, the observed rate constant (k_{obs}) may be given by $k_H K_{et}$, where K_{et} is the equilibrium constant for the endergonic electron transfer and k_H is the rate constant of proton transfer from the radical cation to the dianion in the solvent cage. In such a case, the rate constant of overall hydrogen transfer from NADH analogs to radical anions is determined by the energetics of electron transfer and the rate constant of proton transfer. This is essentially the same as the case of hydride transfer from BNAH to Q, in which the rate constant of overall hydride transfer is determined by the energetics of electron transfer from BNAH to Q and the rate constant of proton transfer from $BNAH^{\cdot +}$ to $Q^{\cdot -}$, because the second electron transfer from $BNA^{\cdot}$ to $QH^{\cdot}$ is highly exergonic (Scheme 2).

FLAVINS

Flavins (Fl) are yellowish tricyclic isoalloxazines that are versatile redox coenzymes in a variety of enzymatic systems (7, 83). Metal ions such as Mg^{2+} and Zn^{2+} ion are known to form complexes with Fl [**1a, 1b,** and **2a–c** (5-deazaflavins)] with a 1:1 stoichiometry in dry MeCN at 298 K (Eq. 11) (23, 26), as is the case of an NADH analog (Eq. 5). The removal of

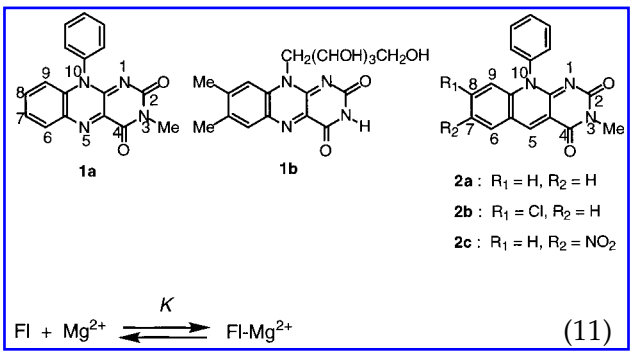

(11)

H_2O from solvent is essential to obtain large formation constants. As such, the addition of small concentrations of H_2O to the Fl-Mg^{2+} system causes a significant decrease in the K value; the K values (1.5×10^2 and $6.5 \times 10\ M^{-1}$ in the presence of 2.8×10^{-2} and $8.3 \times 10^{-2}\ M$ H_2O, respectively) become much smaller than that ($1.7 \times 10^2\ M^{-1}$) in dry MeCN where the H_2O concentration is $< 1 \times 10^{-3}\ M$ (23, 26). In fact, no complex formation of **1a** with Mg^{2+} is observed in H_2O (23, 26). The metal ion interacts with the C2-carbonyl group of Fl, as is evident from the significant red shift of only the C═O stretching bands due to the C2-carbonyl group of **1a** and **2a–c** in the Mg^{2+} complexes (26).

Significant enhancement of the oxidizing ability of the singlet excited states of Fl analogs is observed by the complex formation with metal ions (26). The rate constants of photoinduced electron transfer from electron donors to the Fl–metal ion complexes are much larger than those of free Fl (26). The increase of the oxidizing ability of the singlet excited states of Fl by the complex formation with Mg^{2+} or Zn^{2+} has been evaluated quantitatively as 0.33 ± 0.01 eV for different Fl–metal ion complexes (26).

The complex formation with metal ions not only increases the oxidizing ability of the ground and excited states of Fl, but also stabilizes Fl against irradiation of the visible light to prevent the photodegradation. Taken together, irradiation of the absorption band of a **1a**-Mg^{2+} complex makes it possible to oxidize *p*-methylbenzyl alcohol to *p*-methylbenzaldehyde, whereas irradiation of that of a free Fl **1a** results in no dehydrogenation of *p*-methylbenzyl alcohol. Instead, only the predominant photodegradation occurs (24, 26). The reduced Fl-Mg^{2+} complex, FlH_2-Mg^{2+} produced in the photooxidation of *p*-methylbenzyl alcohol by Fl-Mg^{2+} is readily oxidized by O_2 to regenerate the oxidized form Fl-Mg^{2+} (26). The oxidation of FlH_2-Mg^{2+} by O_2 is also accelerated by Mg^{2+} (19). Thus, Fl-metal ion complexes act as efficient photocatalysts for the dehydrogenation of *p*-methylbenzyl alcohol, as shown in Scheme 7 (26). The photocatalytic dehydrogenation of *p*-methylbenzyl alcohol may be initiated by electron transfer from *p*-methylbenzyl alcohol to the singlet excited state $^1Fl^*$-Mg^{2+}, because the rate constant obtained from the ϕ dependence on the concentration of *p*-methylbenzyl alcohol agrees well with that

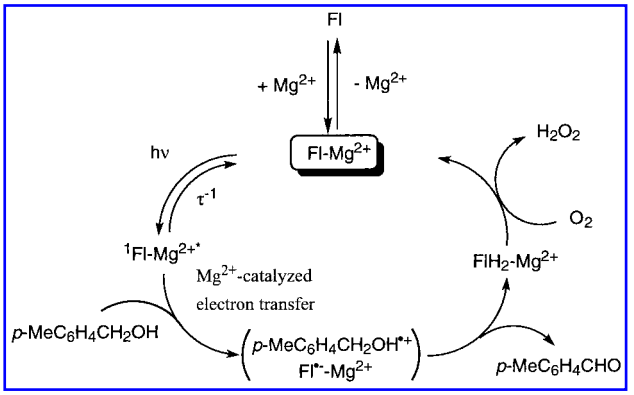

Scheme 7.

obtained independently from the fluorescence quenching of $^1Fl^*\text{-}Mg^{2+}$ (26).

Fl-Mg^{2+} complexes can also catalyze photoinduced oxygenation of R_4Sn via photoinduced electron transfer from R_4Sn to $^1Fl^*\text{-}Mg^{2+}$ in MeCN at 298 K (28). For example, irradiation of an oxygen-saturated MeCN solution containing a Fl analog **1a**-Mg^{2+} complex and Me_4Sn with visible light results in the formation of MeO_2SnMe_3 (Eq. 12) (28). Yields of MeO_2SnMe_3 based on the initial amount of **1a** reach 1,000% in 15 h, indicating that the **1a**-Mg^{2+} complex acts as a photocatalyst in the photoinduced oxygenation of Me_4Sn (28). Neither thermal nor photoinduced oxygenation of Me_4Sn occurs in the absence of the **1a**-Mg^{2+} complex (28).

$$Me_4Sn + O_2 \xrightarrow[Fl\text{-}Mg^{2+}]{h\nu} MeO_2SnMe_3 \qquad (12)$$

PYRROLOQUINOLINE QUINONE (PQQ)

Quinoprotein alcohol dehydrogenases (EC 1.1.99.8) comprise a new class of enzymes that involve a heterocyclic *o*-quinone coenzyme PQQ as a redox catalyst for the enzymatic alcohol-oxidation reactions (1,63). Among them, bacterial methanol dehydrogenase (MDH) is the most well characterized and attractive enzyme that catalyzes the oxidation of methanol to formaldehyde, a key step of the biological C_1-metabolism (1, 2). According to the x-ray structure, there is one calcium ion strongly bound to PQQ through its C-5 quinone carbonyl oxygen, N-6 pyridine nitrogen, and C-7 carboxylate group in the enzyme active site (35, 85). Existence of Ca^{2+} in the enzyme active site has also been suggested for other PQQ-dependent enzymes such as ethanol dehydrogenase from *Pseudomonas aeruginosa* and glucose dehydrogenase from *Acinetobacter calcoaceticus* (4, 34). It has been suggested that Ca^{2+} plays an important role for the structural stabilization of the enzyme (40). The more important role of Ca^{2+} has been shown by the first functional model for MDH, where the calcium complex of a PQQ derivative efficiently oxidizes methanol to formaldehyde (46, 48). So far, binding of Na^+, K^+, Cd^{2+}, Cu^{2+}, and Fe^{3+} to PQQ or its analogs has been examined to demonstrate that the molecular cleft surrounded by the quinone carbonyl group at C-5 (O-5), the pyridine nitrogen (N-6), and the carboxylate group at the 7 position (O-7′) is the most suitable place for the metal ion coordination (42, 68, 76, 82). The 1:1 complex formation of the quinone with Ca^{2+} at C-5 quinone carbonyl oxygen, N-6 pyridine nitrogen, and C-7 methyl ester group has also been confirmed by spectroscopic studies using UV-vis, ^{1}H-NMR, and ^{13}C-NMR (46, 48).

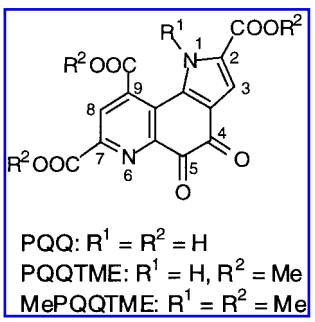

Formation of the C-5 hemiacetal with methanol is significantly enhanced when the quinone is treated with the alcohol in the presence of Ca^{2+}. Addition of a base such as 1,8-diazabicyclo[5.4.0]undec-7-ene (DBU) into a MeCN solution of the PQQTME-Ca^{2+} complex (PQQTME = trimethyl ester of coenzyme PQQ) and methanol leads to the redox reaction to afford reduced PQQTME-Ca^{2+} complex and formaldehyde. Kinetic studies on the redox reaction provided an unequivocal evidence for the addition–elimination mechanism (Scheme 8) (46, 48). The PQQTME-Ca^{2+} complex is shown to act as an efficient catalyst for the oxidation of ethanol to acetaldehyde under aerobic conditions (46, 48).

It has been shown that the binding of Ca^{2+}

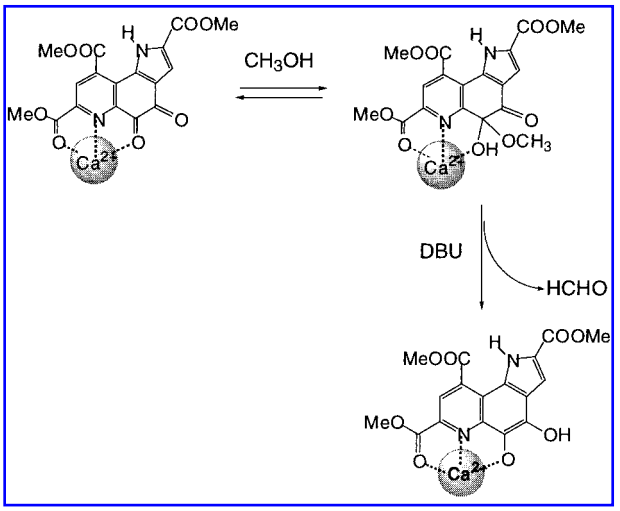

Scheme 8.

to the quinone is much stronger than that of Sr^{2+} and Ba^{2+} (48). This is probably due to the fitting of the metal ions to the molecular cleft of PQQ, because the size of Ca^{2+} fits best to that of the binding pocket of PQQ. The calculated distances using a semiempirical molecular orbital method [Ca^{2+}-O(5′), 2.43 Å, Ca^{2+}-N(6), 2.46 Å, and Ca^{2+}-O(7′); 2.36 Å] of the Ca^{2+}-model complex are all within the range of the reported values for Ca^{2+}—O═C and Ca^{2+}—N_{py} distances in crystals (~2.4 Å) (46,48). Coordination of the larger metal ions, Sr^{2+} and Ba^{2+}, may cause a distortion of the PQQ molecule, making the binding constant K of these metal ions smaller than that of Ca^{2+} (48). Furthermore, addition of an excess amount of a harder Lewis acid such as Mg^{2+} to PQQ resulted in the hydration of the *o*-quinone moiety, causing a deactivation of PQQ for the redox reactions as mentioned above. These facts may be some of the reasons why quinoprotein alcohol dehydrogenases selected Ca^{2+} as a co-catalyst among the alkaline earth metal ions (48).

The enhancement of the oxidizing ability of a PQQ analog by the complexation with Ca^{2+} has been demonstrated by the electrochemical study on PQQTME in aprotic organic solvents (47). The cyclic voltammogram of PQQTME exhibits irreversible redox waves (9). When the pyrrole proton of PQQTME is replaced by a methyl group to give MePQQTME, the cyclic voltammogram of MePQQTME in CH_2Cl_2 exhibits a clearly reversible redox couple at $E_{1/2}$ = −0.90 V versus Fc/Fc^+ (Fc = ferrocene), which corresponds to the one-electron redox couple of MePQQTME/$MePQQTME^{\cdot-}$ (47). It should be noted that the electrochemical behavior of coenzyme PQQ in aprotic organic media is quite similar to that of Fl coenzyme, but PQQ possesses ~0.4 V higher oxidizing ability than Fl cofactor (flavin/flavin semiquinone radical anion couple: −1.3 V versus Fc/Fc^+) (67).

Addition of Ca^{2+} into the solution of MePQQTME causes ~0.57 V positive shift of the one-electron reduction potential of MePQQTME as shown in Fig. 6, which demonstrates the enhancement of the oxidation power of MePQQTME by a strong interaction between Ca^{2+} and $MePQQTME^{\cdot-}$ (47). This indicates that the oxidation power of PQQ in MDH is also enhanced significantly by the Ca^{2+} coordination as compared with free PQQ.

The well resolved solution ESR spectra of $MePQQTME^{\cdot-}$ and $MePQQTME^{\cdot-}$-Ca^{2+} in MeCN can be obtained successfully by using the electrolysis cell with the helical gold wire with large surface area as shown in Fig. 7 (47). Each ESR spectrum can be reproduced perfectly by the computer simulation using hyperfine splitting (hfs) values in which the $\alpha_{N(6)}$ value becomes larger by the complexation with Ca^{2+} and while the other hfs values are not per-

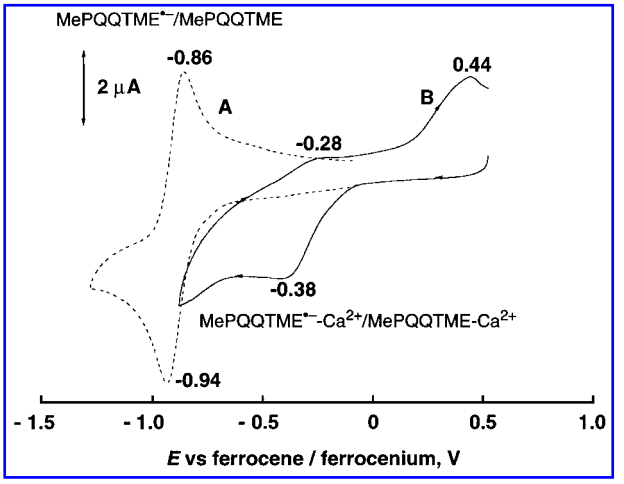

FIG. 6. Cyclic voltammograms of MePQQTME (1.1 m*M*) (trace A) in the absence of $Ca(ClO_4)_2$ and (trace B) in the presence of $Ca(ClO_4)_2$ (1.1 m*M*) in deaerated MeCN at 298 K (47).

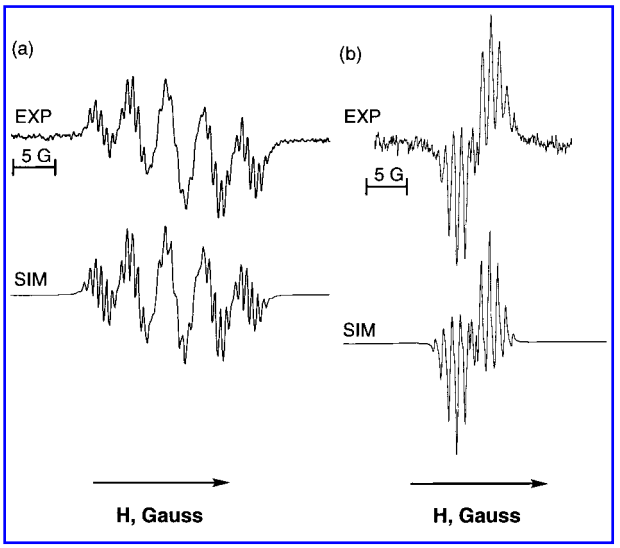

FIG. 7. ESR spectra of (a) MePQQTME$^{\cdot -}$ electrochemically generated at −0.8 V versus Ag/Ag$^+$ in CH_2Cl_2 and (b) MePQQTME$^{\cdot -}$-Ca^{2+} electrochemically generated at −0.8 V versus Ag/Ag$^+$ in the presence of $Ca(ClO_4)_2$ (1 equiv. 1.0 m*M*) in MeCN at 25°C (47).

turbed significantly. This indicates that Ca^{2+} binds to the pyridine nitrogen as in the case of MePQQTME$^{\cdot -}$-Ca^{2+}.

Reoxidation of reduced PQQ to the quinone form by O_2 has also been shown to be enhanced drastically by Ca^{2+} (45). Thus, the oxidation of ethanol to acetaldehyde proceeded catalytically (1,450% based on PQQTME after 65 h), when the reaction was carried out under aerobic conditions (48). In this system, O_2 acts as an electron acceptor to regenerate the quinone from the reduced PQQ.

TRYPTOPHAN TRYPTOPHYLQUINONE (TTQ)

Bacterial methylamine dehydrogenase and aromatic amine dehydrogenase are new members of quinoprotein (quinone-containing enzymes), which involve a heterocyclic *o*-quinone cofactor TTQ at their active sites of the light subunits (64). This cofactor is derived post-translationally from two tryptophan residues in the enzyme active site, acting as the redox catalyst for the enzymatic oxidation of primary amines to the corresponding aldehydes (Eq. 13) (64).

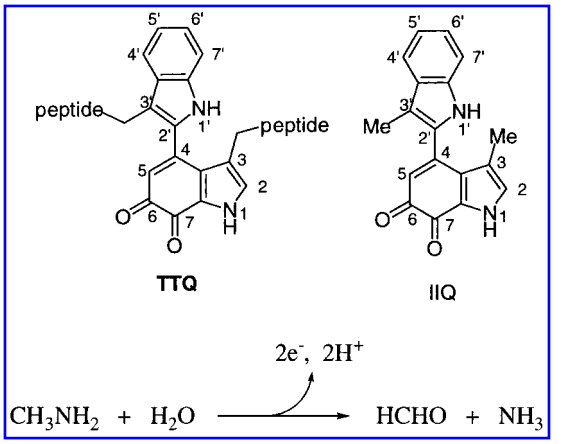

(13)

Monovalent cations such as ammonium ion and alkaline metal ions have recently been shown to influence not only the UV/visible spectrum of the cofactor, but also the reactivity of TTQ in the amine-oxidation reaction and in the electron transfer from the reduced TTQ to amicyanin (6,36,37,58,66). It has been demonstrated that the enzymes have two different cation binding sites, one of which is located near the quinone carbonyl oxygen O(6) of the cofactor. The cationic species incorporated into this binding region have been suggested to interact directly with the quinone, affecting the electronic structure of the cofactor as well as the reactivity in both the amine-oxidation reaction and the subsequent electron-transfer process. It has also been reported that the semiquinone radical of TTQ in the enzyme active site is largely stabilized by the interaction with the cationic species (37).

The extensive data for the visible/near infrared spectra and the binding constants for a series of metal ion complexes of a TTQ model compound [IIQ,1,3-dimethyl-4-(3′-methylindol-2′-yl)indole-6,7-dione] have provided useful clues to identify the cationic species involved in TTQ-dependent enzymes (50,51). The intramolecular charge-transfer bands from the indole ring to the quinone moiety of metal ion-IIQ complexes are highly sensitive to the type of metal ions, and the charge-transfer energies are well correlated with the binding strength of the metal ions to IIQ. For example, the absorption band at 408 nm due to the quinone of IIQ is shifted to 430 nm in the Li^+ complex, and a broad absorption band appears at 626 nm (51). Essentially the same spectral change was ob-

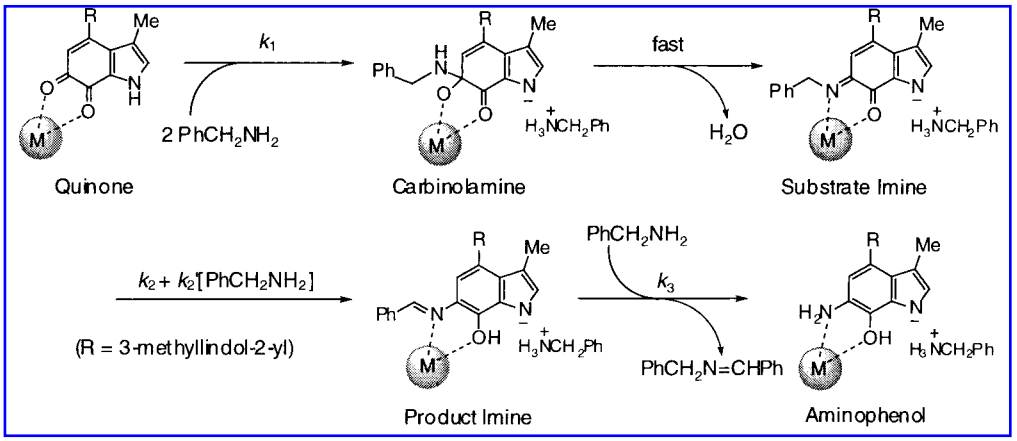

Scheme 9.

served in the titration with $NaClO_4$. The IIQ complexes with divalent metal cations, Mg^{2+} and Ca^{2+}, gave the more red-shifted absorption bands as compared with the monovalent cations (51). The spectral change becomes more prominent for trivalent metal cations, and in particular the Sc^{3+} complex gives the two absorption maxima at 489 and 802 nm, which are the most red-shifted (51). In the presence of an amine substrate, deprotonation of the pyrrole proton takes place to enhance the binding with monovalent and divalent metal ions, whereas the binding strength of trivalent metal ions is reduced by the complexation with the base (51).

The enhancement of the oxidizing ability of TTQ model compounds has been shown by large positive shifts in the one-electron reduction potentials of metal ion–TTQ model complexes as compared with those in the absence of the metal ion (51). For example, addition of Mg^{2+} results in a remarkably large positive shift of E^0_{red} by 1.17 V. In the presence of Sc^{3+}, IIQ also exhibited a reversible redox couple at 0.35 V versus $Ag/AgNO_3$, causing a similar large positive shift of E^0_{red} ($\Delta E^0_{red} = 1.16$ V). This indicates the much stronger binding of IIQ radical anion with metal ions as compared with the neutral compound. The interaction between the radical anion with Mg^{2+} ion is directly detected by the ESR spectrum in comparison with that of the radical anion without metal ion (51). The smaller g value of $IIQ^{\cdot -}$-Mg^{2+} than that of $IIQ^{\cdot -}$(2.0038) indicates that the spin density on oxygen nuclei in $IIQ^{\cdot -}$-Mg^{2+} is decreased by the complexation with Mg^{2+}. The hyperfine structure can be well reproduced by the computer simulation with the hfs values of eight protons, two sets of methyl protons, and two nitrogen atoms (51). It has been shown that the spin densities in $IIQ^{\cdot -}$-Mg^{2+} are significantly decreased by the coordination to Mg^{2+} (51).

Metal ion–TTQ model complexes can oxidize not only benzylamine, but also aliphatic amines in anhydrous organic media, whereas no reaction takes place in the absence of the metal ion under otherwise the same experimental conditions (51). Metal ions are shown to accelerate each step in three distinct steps: the addition of the amine to the quinone, the spontaneous and the amine-catalyzed rearrangement from the substrate imine to the product imine, and the imine exchange reaction to generate the aminophenol and $RCH_2N{=}CHR$ (Scheme 9) (51). Thus, cationic species involved in the enzyme may also act as a catalyst to promote the overall amine oxidation.

SUMMARY AND CONCLUSIONS

As demonstrated in this review, both thermal and photoinduced redox reactions of various coenzyme analogs are accelerated by complexation with metal ions. Such effects of metal ions to enhance the redox reactivities of coenzymes certainly play essential roles in a variety of enzymatic reaction systems involving coenzymes. Quantitative measure to determine

the Lewis acidity of a variety of metal ions described in the beginning of this review, combined with subsequent examples of metal ion-promoted redox reactions of coenzyme analogs, will provide a useful guide to expand the scope of catalytic control of redox reactivities of coenzyme analogs by metal ions.

ACKNOWLEDGMENTS

The authors gratefully acknowledge the contributions of their collaborators and co-workers mentioned in the references (in particular, Dr. T. Suenobu, Dr. K. Ohkubo, and Dr. H. Ohtsu). The authors acknowledge continuous support of their study by a Grant-in-Aid from the Ministry of Education, Culture, Sports, Science and Technology, Japan.

ABBREVIATIONS

$AcrH_2$, 10-methyl-9,10-dihydroacridine; Bdpi, 4,5-bis[di(2-pyridylmethyl)aminomethyl]imidazole; BNAH, 1-benzyl-1,4-dihydronicotinamide; Bu, butyl; DBU, 1,8-diazabicyclo[5.4.0]undec-7-ene; DDQ, 2,3-dicyano-5,6-dichloro-*p*-benzoquinone; $DPPH^{\cdot}$, 1,1-diphenyl-2-picrylhydrazyl; ESR, electron spin resonance; Et, ethyl; Fl, flavin; hfs, hyperfine splitting; IIQ, 1,3-dimethyl-4-(3′-methylindol-2′-yl)indole-6,7-dione; MDH, methanol dehydrogenase; Me, methyl; MeCN, acetonitrile; $MeIM(Py)_2$, (1-methyl-4-imidazolylmethyl)bis(2-pyridylmethyl)amine; M^{n+}, metal ion; NAD^+, nicotinamide adenine dinucleotide; $NADP^+$, nicotinamide adenine dinucleotide phosphate; $O_2^{\cdot -}$, superoxide ion; Ph, phenyl; PQQ, pyrroloquinoline quinone; PQQTME, PQQ trimethyl ester; Q, *p*-benzoquinone; SCE, standard calomel electrode; SOD, superoxide dismutase; TCNE, tetracyanoethylene; TCNQ, 7,7,8,8-tetracyano-*p*-quinodimethan; TPP, tetraphenylporphyrin; TTQ, tryptophan tryptophylquinone.

REFERENCES

1. Anthony C. Methanol dehydrogenase in Gram-negative bacteria. In: *Principles and Applications of Quinoproteins*, edited by Davidson VL. New York, Marcel Dekker, Inc., 1993, pp. 17–45.
2. Anthony C, Ghosh M, and Blake CCF. The structure and function of methanol dehydrogenase and related quinoproteins containing pyrroloquinoline quinone. *Biochem J* 304: 665–674, 1994.
3. Aubert C, Brettel K, Mathis P, Eker APM, and Boussac A. EPR detection of the transient tyrosyl radical in DNA photolyase from *Anacystis nidulans. J Am Chem Soc* 121: 8659–8660, 1999.
4. Bardea A, Katz E, Bückmann AF, and Willner I. NAD^+-dependent enzyme electrodes: electrical contact of cofactor-dependent enzymes and electrodes. *J Am Chem Soc* 119: 9114–9119, 1997.
5. Bertini I, Banci L, Piccioli M, and Claudio L. Spectroscopic studies on copper-zinc-superoxide dismutase (Cu_2Zn_2SOD): a continuous advancement of investigation tools. *Coord Chem Rev* 100: 67–103, 1990.
6. Bishop GR and Davidson VL. Catalytic role of monovalent cations in the mechanism of proton transfer which gates an interprotein electron transfer reaction. *Biochemistry* 36: 13586–13592, 1997.
7. Bruice TC. Mechanisms of flavin catalysis. *Acc Chem Res* 13, 256–262, 1980.
8. Dyrek K and Che M. EPR as a tool to investigate the transition metal chemistry on oxide surfaces. *Chem Rev* 97: 305–331, 1997.
9. Eckert TS, Bruice TC, Gainor JA, and Weinreb SM. Some electrochemical and chemical properties of methoxation and analogous quinoquinones. *Proc Natl Acad Sci U S A* 79: 2533–2536, 1982.
10. Ellerby LM, Cabelli DE, Graden JA, and Valentine JS. Copper-zinc superoxide dismutase: why not pH-dependent? *J Am Chem Soc* 118: 6556–6561, 1996.
11. Fridovich I. Superoxide dismutase. An adaptation to a paramagnetic gas. *J Biol Chem* 264: 7761–7764, 1989.
12. Fridovich I. Superoxide radical and superoxide dismutases. *Annu Rev Biochem* 64: 97–112, 1995.
13. Fukuzumi S. Mechanisms and catalysis in electron transfer chemistry of redox coenzyme analogs. In: *Advances in Electron Transfer Chemistry, Vol. 2*, edited by Mariano PS. Greenwich: JAI Press, 1992, pp. 67–175.
14. Fukuzumi S. Catalysis on electron transfer and the mechanistic insight into redox reactions. *Bull Chem Soc Jpn* 70: 1–28, 1997.
15. Fukuzumi S. Fundamental concepts of catalysis in electron transfer. In: *Electron Transfer in Chemistry*, edited by Balzani V. Weinheim: Wiley–VCH, 2001, Vol. 4, pp. 3–67.
16. Fukuzumi S and Itoh S. Catalysis of photoinduced electron transfer reactions. In: *Advances in Photochemistry, Vol. 25*, edited by Neckers DC, Volman DH, and von Bünau G. New York: Wiley, 1998, pp. 107–172.
17. Fukuzumi S and Ohkubo K. Quantitative evaluation of Lewis acidity of metal ions derived from the *g*-values of ESR spectra of superoxide-metal ion complexes in relation with the promoting effects in electron transfer reactions. *Chem Eur J* 6: 4532–4535, 2000.
18. Fukuzumi S and Okamoto T. Magnesium perchlorate-catalyzed Diels–Alder reactions of anthracenes with *p*-benzoquinone derivatives: catalysis on the electron transfer step. *J Am Chem Soc* 115: 11600–11601, 1993.

19. Fukuzumi S and Okamoto T. Catalysis by magnesium ion of reduction of oxygen by the 1,5-dihydroflavin anion via electron transfer. *J Chem Soc Chem Commun* 521–522, 1994.
20. Fukuzumi S and Tokuda Y. Na^+-catalyzed reduction of semiquinone radical anions by NADH analogues. *Chem Lett* (*Jpn*) 1497–1500, 1992.
21. Fukuzumi S and Yorisue T. Quinone/hydroxide ion induced oxygenation of *p*-benzoquinone to rhodizonate dianion ($C_6O_6^{2-}$), accompanied by the one-electron reduction to semiquinone radical anions. *J Am Chem Soc* 113: 7764–7765, 1991.
22. Fukuzumi S, Kondo Y, and Tanaka T. An inhibitory effect of Mg^{2+} ion by the complex formation with 1-benzyl-1,4-dihydronicotinamide on the reduction of 7,7,8,8-tetracyano-*p*-quinodimethan. *Chem Lett* (*Jpn*) 485–488, 1983.
23. Fukuzumi S, Kuroda S, and Tanaka T. Catalytic effects of Mg^{2+} ion on electron transfer reactions of photo-excited flavin analogues (3-methyl-10-phenyl-5-deazaisoalloxazines and 3-methyl-10-phenylisoalloxazine) with methyl and methoxy substituted benzenes. *Chem Lett* (*Jpn*) 417–420, 1984.
24. Fukuzumi S, Kuroda S, and Tanaka T. Photooxidation of *p*-methylbenzyl alcohol by oxygen, catalyzed by flavin analogues (3-methyl-10-phenylisoalloxazine and 3-methyl-10-phenyl-5-deazaisoalloxazine) in the presence of Mg^{2+} ion. *Chem Lett* (*Jpn*) 1375–1378, 1984.
25. Fukuzumi S, Nishizawa N, and Tanaka, T. Mechanism of hydride transfer from an NADH model compound to *p*-benzoquinone derivatives. *J Org Chem* 49: 3571–3778, 1984.
26. Fukuzumi S, Kuroda S, and Tanaka T. Flavin analogue-metal ion complexes acting as efficient photocatalysts in the oxidation of *p*-methylbenzyl alcohol by oxygen under irradiation with visible light. *J Am Chem Soc* 107: 3020–3027, 1985.
27. Fukuzumi S, Nishizawa N, and Tanaka T. Effects of magnesium(II) ion on hydride-transfer reactions from an NADH model compound to *p*-benzoquinone derivatives. The quantitative evaluation based on the reaction mechanism. *J Chem Soc* [*Perkin 2*] 37–378, 1985.
28. Fukuzumi S, Kuroda S, and Tanaka T. Photoelectron-transfer reaction of flavin analogues with tetraalkyltin compounds. *J Chem Soc* [*Perkin 2*] 25–29, 1986.
29. Fukuzumi S, Koumitsu S, Hironaka K, and Tanaka T. Energetic comparison between photoinduced electron transfer reactions from NADH model compounds to organic and inorganic oxidants, and hydride transfer reactions from NADH model compounds to *p*-benzoquinone derivatives. *J Am Chem Soc* 109: 305–316, 1987.
30. Fukuzumi S, Tokuda Y, Chiba Y, Greci L, Carioni P, and Damiani E. Effect of magnesium ion distinguishing between one-step hydrogen-transfer and electron-transfer mechanisms for the reduction of stable neutral radicals by NADH analogues. *J Chem Soc Chem Commun* 1575–1577, 1993.
31. Fukuzumi S, Tokuda Y, Kitano T, Okamoto T, and Otera J. Electron-transfer oxidation of 9-substituted 10-methyl-9,10-dihydroacridines. Cleavage of C-H vs C-C bond of the radical cations. *J Am Chem Soc* 115: 8960–8968, 1993.
32. Fukuzumi S, Patz M, Suenobu T, Kuwahara Y, and Itoh S. ESR spectra of superoxide anion-scandium complexes detectable in fluid solution. *J Am Chem Soc* 121: 1605–1606, 1999.
33. Fukuzumi S, Ohkubo K, Tokuda Y, and Suenobu T. Hydride transfer from 9-substituted 10-methyl-9,10-dihydroacridines to hydride acceptors via charge-transfer complexes and sequential electron-proton-electron transfer. A negative temperature dependence of the rates. *J Am Chem Soc* 122: 4286–4294, 2000.
34. Geiger O and Görisch H. Quinoprotein ethanol dehydrogenase: preparation of the apo-form and reconstitution with pyrroloquinoline quinone and Ca^{2+} or Sr^{2+} ions. *Agric Biol Chem* 55: 1721–1726, 1991.
35. Ghosh M, Anthony C, Harlos K, Goodwin MG, and Blake C. The refined structure of the quinoprotein methanol dehydrogenase from *Methylobacterium extorquens* at 1.94 Å. *Structure* 3: 177–187, 1995.
36. Gorren ACF and Duine JA. The effects of pH and cations on the spectral and kinetic properties of methylamine dehydrogenase from *Thiobacillus versutus. Biochemistry* 33: 12202–12209, 1994.
37. Gorren ACF, de Vries S, and Duine JA. Binding of monovalent cations to methylamine dehydrogenase in the semiquinone state and its effect on electron transfer. *Biochemistry* 34: 9748–9754, 1995.
38. Guindon Y, Guerin B, Rancourt J, Chabot C, Mackintosh N, and Ogilvie WW. Lewis acids in diastereoselective processes involving acyclic radicals. *Pure Appl Chem* 68: 89–96, 1996.
39. Halfen JA, Jazdzewski BA, Mahapatra S, Berreau LM, Wilkinson EC, Que L, Jr, and Tolman WB. Synthetic models of the inactive copper(II)-tyrosinate and active copper(II)-tyrosyl radical forms of galactose and glyoxal oxidases. *J Am Chem Soc* 119: 8217–8227, 1997.
40. Harris T.K and Davidson VL. Thermal stability of methanol dehydrogenase is altered by the replacement of enzyme-bound Ca^{2+} with Sr^{2+}. *Biochem J* 303: 141–145, 1994.
41. Hughes MN. *The Inorganic Chemistry of Biological Processes*; 2nd ed. New York: John Wiley & Sons, 1984.
42. Ishida T, Doi M, Tomita K, Hayashi H, Inoue M, and Urakami T. Molecular and crystal structure of PQQ (methoxation), a novel coenzyme of quinoproteins: extensive stacking character and metal ion interaction. *J Am Chem Soc* 111: 6822–6828, 1989.
43. Ishikawa M and Fukuzumi S. Primary kinetic isotope effects on acid-catalysed reduction of *p*-benzoquinone derivatives by an acid-stable NADH analogue. *J Chem Soc, Faraday Trans* 86: 3531–3536, 1990.
44. Ito N, Phillips SEV, Stevens C, Ogel ZB, McPherson MJ, Keen JN, Yadav KDS, and Knowles PF. Novel thioether bond revealed by 1.7 Å crystal structure of galactose oxidase. *Nature* 350: 87–90, 1991.
45. Itoh S, Kawakami H, and Fukuzumi S. Catalysis by calcium ion of the reoxidation of reduced PQQ by molecular oxygen. *Chem Commun* 29–30.

46. Itoh S, Kawakami H, and Fukuzumi S. Modeling of the chemistry of quinoprotein methanol dehydrogenase. Oxidation of methanl by calcium complex of coenzyme PQQ via addition–elimination mechanism. *J Am Chem Soc* 119: 439–440, 1997.
47. Itoh S, Kawakami H, and Fukuzumi S. Electrochemical behavior and characterization of semiquinone radical anion species of coenzyme PQQ in aprotic organic media. *J Am Chem Soc* 120: 7271–7277, 1998.
48. Itoh S, Kawakami H, and Fukuzumi S. Model studies on calcium-containing quinoprotein alcohol dehydrogenases. Catalytic role of Ca^{2+} for the oxidation of alcohols by coenzyme PQQ (4,5-dihydro-4,5-dioxo-1*H*-pyrrolo[2,3-*f*]quinoline-2,7,9-tricarboxylic acid). *Biochemistry* 37: 6562–6571, 1998.
49. Itoh S, Taki M, and Fukuzumi S. Active site models for galactose oxidase and related enzymes. *Coord Chem Rev* 198: 3–20, 2000.
50. Itoh S, Taniguchi M, and Fukuzumi S. Catalytic effect of monovalent cations on the amine-oxidation by cofactor TTQ of quinoprotein amine dehydrogenases. *Chem Commun* 329–330, 2000.
51. Itoh S, Taniguchi M, Takada N, Nagatomo S, Kitagawa T, and Fukuzumi S. Effects of metal ions on the electronic, redox, and catalytic properties of cofactor TTQ of quinoprotein amine dehydrogenases *J Am Chem Soc* 122: 12087–12097, 2000.
52. Itoh S, Kumei H, Nagatomo S, Kitagawa T, and Fukuzumi S. Effects of metal ions on physicochemical properties and redox reactivity of phenolates and phenoxyl radicals. Mechanistic insight into hydrogen atom abstraction by phenoxyl radical-metal complexes. *J Am Chem Soc* 123: 2165–2175, 2001.
53. Ivancich A, Jouve HM, and Gaillard J. EPR evidence for a tyrosyl radical intermediate in bovine liver catalase. *J Am Chem Soc* 118: 12852–12853, 1996.
54. Kaim W and Schwederski B. *Bioinorganic Chemistry: Inorganic Elements in the Chemistry of Life*, New York: John Wiley & Sons, 1994.
55. Känzig W and Cohen MH. Paramagnetic resonance of oxygen in alkali halides. *Phys Rev Lett* 3: 509–510, 1959.
56. Kasai PH. Electron spin resonance studies of γ- and x-ray-irradiated zeolites. *J Chem Phys* 43: 3322–3327, 1965.
57. Kessar SV and Singh P. Lewis acid complexation of tertiary amines and related compounds: a strategy for α-deprotonation and stereocontrol. *Chem Rev* 97: 721–737, 1997.
58. Kuusk V and McIntire WS. Influence of monovalent cations on the ultraviolet-visible spectrum of tryptophan tryptophylquinone-containing methylamine dehydrogenase from bacterium W3A1. *J Biol Chem* 269: 26136–26143, 1994.
59. Lippard SJ and Berg JM. *Principles of Bioinorganic Chemistry*. Mill Valley, CA: University Science Books, 1994.
60. Lunsford JH. ESR of adsorbed oxygen species. *Catal Rev* 8: 135–157, 1973.
61. MacMillan F, Kannt A, Behr J, Prisner T, and Michel H. Direct evidence for a tyrosine radical in the reaction of cytochrome *c* oxidase with hydrogen peroxide. *Biochemistry* 38: 9179–9184, 1999.
62. Mahrwald R. Diastereoselection in Lewis-acid-mediated aldol additions. *Chem Rev* 99: 1095–1120, 1999.
63. Matsushita K and Adachi O. Bacterial quinoproteins glucose dehydrogenase and alcohol dehydrogenase. In: *Principles and Applications of Quinoproteins*, edited by Davidson VL. New York: Marcel Dekker, Inc., 1993, pp. 47–63.
64. McIntire WS, Wemmer DE, Chistoserdov A, and Lidstrom ME. A new cofactor in a prokaryotic enzyme: tryptophan tryptophylquinone as the redox prosthetic group in methylamine dehydrogenase. *Science* 252: 817–824, 1991.
65. Mero CL and Porter NA. Lewis acid-promoted atom-transfer free radical additions. *J Am Chem Soc* 121: 5155–5160, 1999.
66. Moenne-Loccoz P, Nakamura N, Itoh S, Fukuzumi S, Gorren ACF, Duine JA, and Sanders-Loehr J. Electronic environment of the tryptophylquinone cofactor in methylamine dehydrogenase. Evidence from resonance Raman spectroscopy of model compounds. *Biochemistry* 35: 4713–4720, 1996.
67. Niemz A, Imbriglio J, and Rotello VM. Model systems for flavoenzyme activity: one- and two-electron reduction of flavins in aprotic hydrophobic environments. *J Am Chem Soc* 119: 887–892, 1997.
68. Noar JB, Rodriguez EJ, and Bruice TC. Synthesis of 9–decarboxymethoxatin. Metal complexation of methoxation as a possible requirement for its biological activity. *J Am Chem Soc* 107: 7198–7199, 1985.
69. Ohtsu H and Fukuzumi S. The essential role of a Zn(II) ion in the disproportionation reaction of semiquinone radical anion by an imidazolate-bridged Cu(II)-Zn(II) model of superoxide dismutase. *Angew Chem Int Ed Engl* 39: 4537–4539, 2000.
70. Ohtsu H, Itoh S, Nagatomo S, Ogo S, Kitagawa T, Watanabe Y, and Fukuzumi S. Characterization of imidazolate-bridged Cu(II)-Zn(II) heterodinuclear and Cu(II)-Cu(II) homodinuclear hydroperoxo complexes as reaction intermediate models of Cu,Zn-SOD. *Chem Commun* 1051–1052, 2000.
71. Ohtsu H, Shimazaki Y, Odani A, Yamauchi O, Itoh S, and Fukuzumi S. Synthesis and characterization of imidazolate-bridged dinuclear complexes as active site models of Cu,Zn-SOD. *J Am Chem Soc* 122: 5733–5741, 2000.
72. Renaud P and Gerster M. Use of Lewis acids in free radical reactions. *Angew Chem Int Ed Engl* 37: 2562–2579, 1998.
73. Santelli M and Pons JM. *Lewis Acids and Selectivity in Organic Synthesis*. Boca Raton, FL: CRC Press, 1995.
74. Sawyer DT, Calderwood TS, Yamaguchi K, and Angelis CT. Synthesis and characterization of tetramethylammonium superoxide. *Inorg Chem* 22: 2577–2583, 1983.
75. Schinzer D (Ed). *Selectivities in Lewis Acid Promoted Reactions*. Dordrecht, The Netherlands: Kluwer Academic Publishers, 1989.

76. Schwederski B, Kasack V, Kaim W, Roth E, and Jordanov J. Ambident behavior of the "new vitamin" methoxatin (cofactor PQQ) towards metals: coordinative stabilization of the pyrrolide form and the semiquinone form. *Angew Chem Int Ed Engl* 29: 78–79, 1990.
77. Sibi MP, Ji J, Sausker JB, and Jasperse CP. Free radical-mediated intermolecular conjugate additions. Effect of the Lewis acid, chiral auxiliary, and additives on diastereoselectivity. *J Am Chem Soc* 121: 7517–7526, 1999.
78. Sigman DS, Hajdu J, and Creighton DJ. Nonenzymic dihydronicotinamide reductions as probes for the mechanism of NAD^+-dependent dehydrogenases. In: *Bioorganic Chemistry*, edited by van Tamelen EE. New York: Academic Press, 1978, Vol. IV, pp. 385–407.
79. Sokolowski A, Müller J, Weyhermüller T, Schnepf R, Hildebrandt P, Hildenbrand K, Bothe E, and Wieghardt K. Phenoxyl radical complexes of zinc(II). *J Am Chem Soc* 119: 8889–8900, 1997.
80. Stryer L. Biochemistry, 3rd edit. New York: Freeman, 1988, Chap. 17.
81. Stubbe J and van der Donk WA. Protein radicals in enzyme catalysis. *Chem Rev* 98: 705–762, 1998.
82. Suzuki S, Sakurai T, Itoh S, and Ohshiro Y. Preparation and characterization of ternary copper(II) complexes containing coenzyme PQQ and bipyridine or terpyridine. *Inorg Chem* 27: 591–592, 1988.
83. Walsh C. Flavin coenzymes: at the crossroads of biological redox chemistry. *Acc Chem Res* 13: 148–155, 1980.
84. Whittaker MM, Ballou DP, and Whittaker JW. Kinetic isotope effects as probes of the mechanism of galactose oxidase. *Biochemistry* 37: 8426–8436, 1998.
85. Xia Z, Dai W, Zhang Y, White SA, Boyd GD, and Mathews FS. Determination of the gene sequence and the three-dimensional structure at 2.4 Å resolution of methanol dehydrogenase from *Methylophilus* W3A1. *J Mol Biol* 259: 480–501, 1996.
86. Yamamoto H. *Lewis Acid Chemistry: A Practical Approach.* Oxford: Oxford University Press, 1999.
87. Zeller HR and Känzig W. The electronic structure of the superoxide ion-centers in alkali metal halides. I. Paramagnetic and optical spectra and their interpretation. *Helv Phys Acta* 40: 845–872, 1967.

Address reprint requests to:
Shunichi Fukuzumi
Department of Material and Life Science
Graduate School of Engineering
Osaka University
CREST, JAPAN Science and Technology Corporation
2-1 Yamada-oka, Suita
Osaka 565-0871, Japan

E-mail: fukuzmi@ap.chem.eng.osaka-u.ac.jp

Received for publication October 7, 2000; accepted February 25, 2001.

This article has been cited by:

1. Shazia Tanvir, Francois Oudet, Sylviane Pulvin, William A. Anderson. 2012. Coenzyme based synthesis of silver nanocrystals. *Enzyme and Microbial Technology* **51**:4, 231-236. [CrossRef]
2. Shunichi Fukuzumi. 2012. Electron-transfer properties of high-valent metal-oxo complexes. *Coordination Chemistry Reviews* . [CrossRef]
3. Jiyun Park, Yuma Morimoto, Yong-Min Lee, Wonwoo Nam, Shunichi Fukuzumi. 2012. Proton-Promoted Oxygen Atom Transfer vs Proton-Coupled Electron Transfer of a Non-Heme Iron(IV)-Oxo Complex. *Journal of the American Chemical Society* 120216153653005. [CrossRef]
4. Shunichi Fukuzumi, Kei Ohkubo, Yuma Morimoto. 2012. Mechanisms of metal ion-coupled electron transfer. *Physical Chemistry Chemical Physics* **14**:24, 8472. [CrossRef]
5. Jiyun Park, Yuma Morimoto, Yong-Min Lee, Youngmin You, Wonwoo Nam, Shunichi Fukuzumi. 2011. Scandium Ion-Enhanced Oxidative Dimerization and N -Demethylation of N , N -Dimethylanilines by a Non-Heme Iron(IV)-Oxo Complex. *Inorganic Chemistry* 111024010100009. [CrossRef]
6. Shunichi FukuzumiProton-Coupled Electron Transfer in Hydrogen and Hydride Transfer Reactions 39-74. [CrossRef]
7. Shunichi Fukuzumi, Kei Ohkubo. 2010. Metal ion-coupled and decoupled electron transfer. *Coordination Chemistry Reviews* **254**:3-4, 372-385. [CrossRef]
8. Shunichi Fukuzumi, Hiroaki Kotani, Tomoyoshi Suenobu, Seungwoo Hong, Yong-Min Lee, Wonwoo Nam. 2010. Contrasting Effects of Axial Ligands on Electron-Transfer Versus Proton-Coupled Electron-Transfer Reactions of Nonheme Oxoiron(IV) Complexes. *Chemistry - A European Journal* **16**:1, 354-361. [CrossRef]
9. Junpei Yuasa, Shunichi Fukuzumi. 2008. A mechanistic dichotomy in concerted versus stepwise pathways in hydride and hydrogen transfer reactions of NADH analogues. *Journal of Physical Organic Chemistry* **21**:10, 886-896. [CrossRef]
10. Shunichi Fukuzumi. 2008. Metal Ion-coupled Electron-transfer Reduction of Dioxygen. *Chemistry Letters* **37**:8, 808-813. [CrossRef]
11. David G Kehres, Michael E Maguire. 2003. Emerging themes in manganese transport, biochemistry and pathogenesis in bacteria. *FEMS Microbiology Reviews* **27**:2-3, 263-290. [CrossRef]